2021-05-01

High Frequency Electron Spin Resonance Investigations On Quasi-Two-Dimensional Chromium Halide Magnets

Christian Saiz
University of Texas at El Paso

HIGH FREQUENCY ELECTRON SPIN RESONANCE INVESTIGATIONS ON QUASI-TWO-DIMENSIONAL CHROMIUM HALIDE MAGNETS

CHRISTIAN LEE SAIZ

Master's Program in Physics

APPROVED:

Srinivasa Rao Singamaneni, Ph.D., Chair

Rosa Fitzgerald, Ph.D.

Sreeprasad T. Sreenivasan, Ph.D.

Stephen L. Crites, Jr., Ph.D.
Dean of the Graduate School

DEDICATION

To every single member of my family, my friends, and loved ones who stood with and pushed me through my educational journey. To my mother and father: Your love, support and words of encouragement have never left me. And to Frankie: I couldn't have done this without your endless support.

HIGH FREQUENCY ELECTRON SPIN RESONANCE INVESTIGATIONS ON QUASI-TWO-DIMENSIONAL CHROMIUM HALIDE MAGNETS

by

CHRISTIAN LEE SAIZ, B.S.

THESIS

Presented to the Faculty of the Graduate School of

The University of Texas at El Paso

in Partial Fulfillment

of the Requirements

for the Degree of

MASTER OF SCIENCE

Department of Physics

THE UNIVERSITY OF TEXAS AT EL PASO

May 2021

ACKNOWLEDGEMENTS

I would like to thank Dr. Srinivasa Rao Singamaneni for the opportunity to work alongside him for over five years. Over the years he has presented me with many opportunities to push myself further and encouraged me to become a better researcher, student, and scientist. I am thankful to all of our collaborators around the United States who have provided invaluable support in supplying samples, conducting measurements, and performing specific data analyses that were crucial in completing the studies presented here. I thank Dr. Fazel Tafti and Thomas Tartaglia at Boston College, who supplied the $CrBr_3$ samples and conducted magnetic measurements while providing important support in the analysis of their data. I thank Dr. Michael A. McGuire from Oak Ridge National Laboratory for supplying the $CrCl_3$ and CrI_3 samples. I thank Dr. Johan van Tol from the National High Magnetic Field Laboratory at Florida State University for conducting all high frequency electron spin resonance spectroscopy experiments. I would also like to thank all of my wonderful coworkers in our laboratory that I have worked with over the years; Henry Alfaro, Daniel Alvarado, Czarena Bush, Dawn Star Blazer, Adrian Cosio, Jose A. Delgado, Hector Iturriaga, Jonathan Landeros, Luis M. Martinez, Samir Muniz, Rubyann Olmos, Monica Teran, who have always extended a helping hand. I would like to thank Jose A. Delgado, who helped author a manuscript focusing on $CrBr_3$, where he aided in the analysis of our EPR data and helped improve all studies presented here.

ABSTRACT

Broadening the knowledge and understanding on the magnetic correlations in van der Waals layered magnets is critical in realizing their potential next-generation applications in devices such as spintronics. In this study, we employ high frequency (ν = 120 GHz, 240 GHz) electron spin resonance (ESR) spectroscopy on plate-like CrX_3 (where X = Cl, Br, I) to gain insight into the magnetic interactions as a function of temperature (200 – 4.4 K) and the angle of rotation θ (degrees). We find that the temperature dependence of the ESR linewidth is well described by the Ginzburg-Landau critical model, indicative of antiferromagnetic correlations and the presence of two-dimensional (2D) correlations. Furthermore, our findings show that the resonance field in CrX_3 follows a $(3\cos^2\theta - 1)$-like angular dependence, while the linewidth follows a $(3\cos^2\theta - 1)^2$-like angular dependence, a behavior indicative of 2D correlations that is likely due to the interaction of the external magnetic field applied during the ESR experiment. The external magnetic field presumably induces an interaction between the long-range spin vortices and spin clusters that may have formed during magnetic phase separation, as evidenced from the bifurcation between zero-field- and field-cooled temperature dependent magnetic susceptibility measurements performed on $CrBr_3$, further confirming the coexistence of antiferromagnetism and ferromagnetism in the bulk compound. Frequency dependent ESR measurements performed on $CrCl_3$ shows a frequency dependence of the ESR linewidth and BKT transition temperature, T_{BKT}, indicative of magnetic field induced behavior in the system. This study demonstrates the significance of employing spin sensitive techniques such as ESR to better understand the magnetic correlations in similar van der Waals magnets.

TABLE OF CONTENTS

LIST OF TABLES

LIST OF FIGURES

PART I: MOTIVATION AND EXPERIMENTAL DETAILS

CHAPTER 1: MOTIVATION

Electron spin resonance (ESR) spectroscopy is an ideal tool to study the magnetic interactions and magnetic anisotropy in van der Waals (vdW) magnetic materials [1-5]. For instance, through the use of high-frequency (ν = 240 GHz) ESR spectroscopy, Lee and co-authors have reported on the fundamental spin interactions that cause the magnetic anisotropy in CrI_3 [1]. In another study, ESR spectroscopy was carried out at various frequencies in the presence of a high magnetic field in order to investigate the magnetic anisotropy in another vdW magnet $Cr_2Ge_2Te_6$ [2]. In another recent work, Zeisner and co-authors used high-field ESR spectroscopy over a range of frequencies to prove the existence of ferromagnetic short-range correlations above the magnetic phase transition and established the intrinsically two-dimensional (2D) nature of the magnetism in $CrCl_3$ [3]. Of significant relevance, through numerous ESR studies on the spin dynamics of the 2D triangular Cr- antiferromagnetic frustrated lattices $ACrO_2$ (where A = Li, Na, Cu, Ag), Hemmida *et al.* have determined that there exists a dominant role of magnetic vortices for the spin relaxation in $ACrO_2$ and call for further investigations on similar compounds [6-9]. Additionally, our group has employed light-induced ESR spectroscopy to study the photoexcited magnetic interactions in CrI_3 and $CrCl_3$ [5].

While numerous ESR works have been carried out on two compounds of the CrX_3 family (CrI_3 and $CrCl_3$), to our knowledge, there has been only a few ESR works reported on $CrBr_3$ in the last 50 years [10,11]. However, the temperature dependence of the ESR linewidth, as well as the angular dependence of the ESR resonance field and linewidth have not been discussed in detail. The temperature and angular dependences of the ESR spectral parameters, such as signal width

and resonance field, provide fingerprint-like signatures of magnetic phase transitions as well as information on microscopic magnetic interactions, which appears to be missing from the literature.

Several decades ago a few ESR studies conducted at and below room temperature (300 K) appeared in the literature on CrI_3 and $CrCl_3$ [10,12,13]. Interest in such materials was recently rejuvenated when long-range magnetic order in pristine 2D crystals $Cr_2Ge_2Te_6$ and CrI_3 [14], as well as the discovery of 2D ferromagnetism in the CrI_3 monolayer, were first reported [15]. This renewed interest in compounds with similar magnetic and structural properties. In addition, to our knowledge, there have been no new reports using ESR on these compounds since 1991, where Chehab *et al.* studied the temperature dependence of the ESR signal coming from $CrCl_3$, confirming that, when a field of the order of H = 3,000 G is applied, $CrCl_3$ exhibits magnetic properties characteristic of a 2D system [13]. To broaden the knowledge and understanding, in addition to performing ESR at ν = 240 GHz to study the angular dependence of the resonance field and linewidth, we have also studied the ESR spectral behavior above room temperature on $CrCl_3$ and CrI_3 single crystals, where the magnetic field was applied within the plane of the sample layers. Here, the magnetic phase transition in the $CrCl_3$ compound as a function of temperature from 5 – 289 K at ν = 120 GHz was also studied by tracking the temperature dependences of signal behavior, signal width, and *g*-value. The change in magnitude in the *g*-value gives information on the atomic or molecular orbital where the unpaired electron is contained, the *g*-factor obtained from the resonance line reflects the strength of microscopic spin-orbit coupling. We also track the changes to the linewidth (full width at half maximum, ΔH) as it is directly connected to the interactions of the spins with their local environment. These works also compare the ESR spectral properties of $CrCl_3$ and CrI_3 as a function of temperature and microwave frequency, which was unreported previously [16].

Since the magnetic resonance properties of bulk CrX_3 serve as a basis for the understanding of magnetic phenomena in reduced dimensions, e.g., in few- or monolayer samples of CrX_3, a profound understanding of magnetic correlations in CrX_3 is needed, especially considering that magnetic mono/few-layers of CrX_3 have now become accessible. Here, through the use of high frequency (ν = 240 GHz) ESR spectroscopy, we show that the temperature dependence of the ESR linewidth, reflective of spin dynamics, follows the Ginzberg-Landau critical model satisfactorily, giving critical exponents indicative of two-dimensionality in bulk $CrBr_3$. In addition, we find that the BKT transition model is not applicable due to the absence of magnetic phase separation. We also find that the angular dependence of the linewidth and resonance field from $CrBr_3$ point toward 2D correlations within the sample, though the precise origin is yet to be resolved.

CHAPTER 2: EXPERIMENTAL DETAILS

2.1 Synthesis Method

CrX_3 single crystals were prepared using the chemical vapor transport (CVT) method as previously reported by our collaborators at Boston College ($CrBr_3$) and Oak Ridge National Laboratory ($CrCl_3$, CrI_3) [17-19]. In this method, a condensed phase material is volatized in the presence of a reactant, in this case a gaseous transport agent, and is "transported" elsewhere allowing for the formation of a crystal. This reaction takes place in a glass or ceramic apparatus, typically a tube, where the elements and transport agent are subjected to a temperature gradient and an external temperature is applied in order to induce volatilization and crystallization. These parameters will vary by element. The temperature gradient will allow for the now gaseous element to be deposited in an area of the tube which is most favorable for it to reach equilibrium and crystallize. [20] A schematic of the setup can be seen in **Figure 2.1**. Such a synthesis method is ideal for producing high quality single crystals with minimal crystal defects.

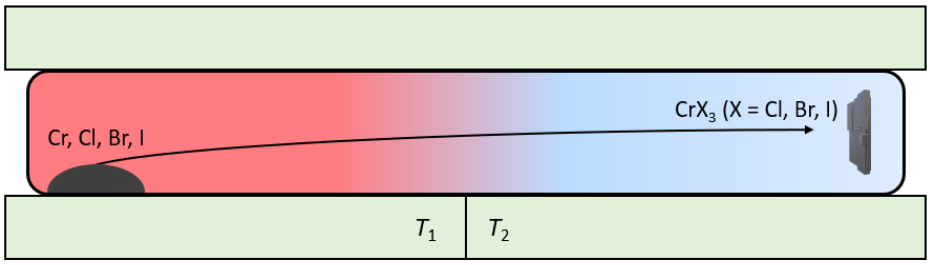

Figure 2.1: CVT setup showing the tube within a temperature gradient where $T_1 > T_2$.

2.2 Properties of CrX_3

Among various van der Waals (vdW) magnets, CrX_3 (where X = Cl, Br, I) is a family of compounds that has gained considerable attention due to their cleavable nature due to weak van

der Waals forces between layers and persistent magnetic properties even at the atomic limit [15,21-24]. The cleavable crystals are semiconducting (CrI_3) and insulating ($CrCl_3$, $CrBr_3$) and, because of these unique magnetic properties, are currently being actively researched for next-generation spintronic and magnetoelectronic applications [15,25-30]. By the nature of their crystal structures, these compounds are strongly anisotropic with magnetic behaviors determined by a weak interlayer coupling, single ion anisotropy and intralayer coupling [31]. By taking advantage of these couplings, researchers have shown that it is possible to electrically control the magnetic behavior of CrI_3 monolayer and bilayers [25]. Particularly, CrX_3 is shown to be a good contender for tunable and cleavable magnetic materials [19,32,33]. In these compounds, magnetism arises from the Cr^{3+} ion (S = 3/2, spin-only contribution) which are arranged in a honeycomb network and are located at the centers of edge-sharing octahedra of six halogen atoms. In quasi-2D/bilayer magnets, the intralayer magnetic (spin) coupling is stronger compared to interlayer. That is because the distance between the Cr atoms is smaller within the layer compared to across the layer. The coupling is through the super exchange interaction through Cr-X-Cr path causing the magnetic order. **Figure 2.2** shows the CrX_3 unit cell and the monolayer atomic structure. CrI_3 is an out-of-plane ferromagnet with a Curie temperature (T_C) of 61 K, while $CrCl_3$ is an in-plane ferromagnet and out-of-plane antiferromagnet with an ordering temperature (Néel temperature, T_N) near 17 K [10,19,34,35]. Similar to CrI_3, $CrBr_3$ is a soft out-of-plane ferromagnetic insulator with T_C = 33 K [24,36] where the easy axis of magnetization lies along the *c*-axis and has been reported to show spontaneous magnetization down to the monolayer [37-39].

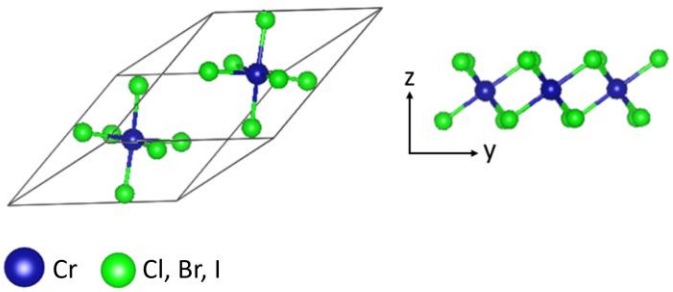

Figure 2.2: Triangular CrX_3 unit cell and a side view of the monolayer atomic structure.

$CrBr_3$ and CrI_3 are interesting platforms to study magnetic interactions due to their changing magnetic properties depending on the number of layers present or the stacking order. Atomically thin $CrBr_3$ has been shown to exhibit ferromagnetic interlayer coupling [40], and recent spin-polarized scanning tunneling microscopy and spectroscopy studies have confirmed this coupling to either be ferromagnetic or antiferromagnetic in the bilayer depending on the stacking order [21]. Conversely, in CrI_3 ferromagnetism perpendicular to the two-dimensional (2D) plane persists down to the monolayer and bilayer CrI_3 shows interlayer antiferromagnetism [21]. $CrCl_3$ differs from the other members of the CrX_3 family in that it has be shown to possess a few unique magnetic transitions. At T_N = 17 K, $CrCl_3$ is an in-plane ferromagnet and out-of-plane antiferromagnet, meaning that the moments lying along the plane defined by the Cr layers are aligned ferromagnetically within a layer, while there is antiferromagnetic order between Cr layers [32]. According to Zeisner *et al.*, there has also been detections of a two-step transition to a long-range ordered state in $CrCl_3$, indicating that $CrCl_3$ is of 2D nature at $T_C \sim 17$ K and enters into a three-dimensional (3D) antiferromagnetically ordered state at $T_N \sim 14$ K [3]. These are all good indicators of magnetic frustration within CrX_3. This series also undergoes a first order crystallographic phase transition at various temperatures upon warming. At ~ 240 K $CrCl_3$

undergoes a phase transition from rhombohedral ($R\bar{3}$) at low temperatures to monoclinic (C2/*m*) at high temperatures [32,41]. CrI_3 undergoes this same first order phase transition at ~ 210 – 220 K [19]. While $CrBr_3$ will also undergo this crystallographic phase transition, it is at a higher temperature of ~ 420 K, meaning that $CrBr_3$ will have a rhombohedral structure at room temperature [19].

With the increase in halogen atom radius, i.e. Cl < Br < I, CrX_3 shows a larger vdW gap, a smaller cleavage energy and a larger in-plane nearest-neighbor Cr-Cr distance, which is why the magnetic phase transition temperature increases with ionic radius and is the reason CrX_3 shows a weaker direct exchange with increasing halogen atom radius [30,32,33,38,42]. Lin *et al.* also suggests that CrX_3 may experience a magnetic phase transition from a 2D-Heisenberg ferromagnet to 3D-Ising behavior as you move from Cl to Br to I [42]. Increasing the atomic radius of the X atom is also expected to increase spin-orbit coupling, which, according to McGuire *et al.*, is a source of magnetic anisotropy in CrX_3 [32].

2.3 Electron Spin Resonance Spectroscopy

2.3.1 Overview

Electron spin resonance (ESR) spectroscopy is a spectroscopic tool in which the sample is subjected to an external magnetic field and microwave radiation in the GHz range. When the sample is exposed to the external magnetic field B_0, the unpaired electrons within the sample will interact with the field according to the Zeeman effect, resulting in a splitting in the energy levels given by $h\nu = \Delta E = g\mu_B B_0$, where g is the spectroscopic g-factor, or Landé g-factor (g-value), and μ_B is the Bohr magneton (**Figure 2.3**). When the energy of the microwave frequency resonates with the energy of this splitting, a photon is absorbed, and the absorption is recorded. This absorption is also called the resonance field. The derivative of the absorption with respect to the

applied field (dP/dH) allows for the extrapolation of the *g*-value, ESR resonance field (H_{res}), and ESR linewidth, all of which give important information on the local magnetic nature, magnetic phase transitions and magnetic interactions within the sample. ESR spectroscopy is most commonly performed using X-band ($\nu \sim 9.4$ GHz) radiation while higher frequencies, such as ν = 120 – 240 GHz used in these experiments, are utilized for higher resolution of the ESR signals, an increased *g*-value resolution, and the ability to study high-spin species that would otherwise be ESR "silent".

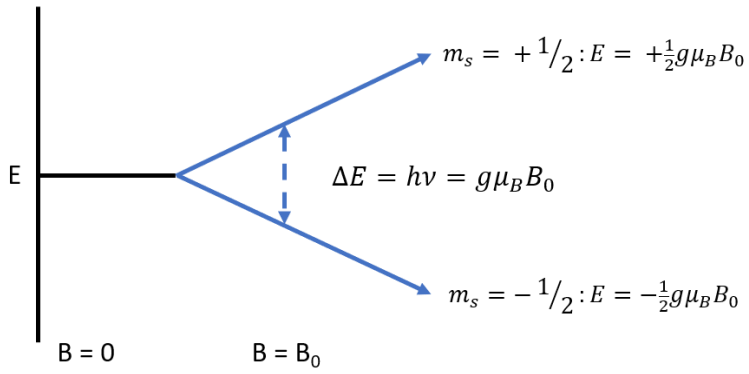

Figure 2.3: Zeeman splitting as a function of applied magnetic field.

2.3.2 Temperature Dependence

Here, through the use of high frequency (ν = 240 GHz) ESR spectroscopy on CrX_3, we show that the temperature dependence of the ESR linewidth, reflective of spin dynamics, follows the Berezinskii-Kosterlitz-Thouless (BKT) transition model satisfactorily, while the Ginzburg-Landau critical model gives critical exponents which describe the magnetic interactions within the bulk systems. The BKT transition is a topological phase transition previously understood to be unique to the 2D *XY* model and can be observed in several 2D systems approximated by the *XY* model such as Josephson junctions [23]. Together Kosterlitz and Thouless, then subsequently

Berezinskii, concluded that a topological phase transition due to the binding and unbinding of magnetic vortices took place at the BKT transition temperature of $T_{BKT} \neq 0$ [43-45]. The temperature dependence of the ESR linewidth and resonance field provides fingerprint-like signatures of magnetic phase transitions as well as information on microscopic magnetic interactions.

2.3.3 Angular Dependence

In these studies, we find that the angular dependence of the linewidth and resonance field from CrX_3 point toward 2D correlations within the family of compounds, attributed to the possible coexistence of ferromagnetism and antiferromagnetism within the system. This is done by fitting our ESR data to the following equations:

$$\mathrm{H_{res}}(\theta) = \mathrm{F}(3\cos^2\theta - 1) + \mathrm{G} \qquad (3)$$

$$\Delta\mathrm{H}(\theta) = \mathrm{A}(3\cos^2\theta - 1)^2 + \mathrm{B} \qquad (4)$$

We find that the resonance field follows a $(3cos^2\theta - 1)$-like angular dependence when the data is fitted to Eq. 3, while the linewidth follows a $(3cos^2\theta - 1)^2$-like angular dependence when fitted with Eq. 4, a behavior indicative of 2D correlations that may be due to the interaction of the external magnetic field applied during the ESR experiment [46,47]. The angular dependence of the ESR spectral parameters such as signal width and resonance field, just as the temperature dependence, provides unique signatures of magnetic phase transitions and information on microscopic magnetic interactions.

2.3.4 Frequency Dependence

We have conducted frequency dependent studies on $CrCl_3$ at ν = 120 GHz and 240 GHz in order to track the change in linewidth under different applied fields. It has been reported by Ashoka

et al. that the BKT transition may be taking place on similar Cr^{3+}-doped compounds due to an effective 2D *XY* easy plane anisotropy induced by the applied magnetic field in the experiment that may induce an interaction between the long-range spin vortices and spin clusters that may have been formed during magnetic phase segregation [46]. In a separate study, these authors tested the hypothesis that the applied EPR field is responsible for the onset of BKT-like behavior and have showed that a higher applied field allows for a higher temperature onset of the threshold anisotropy required for BKT behavior which will manifest as a higher T_{BKT} [47]. In another work, Seehra *et al.* found that the ESR linewidth in $CrBr_3$ shows differing behaviors as a function applied field [11]. Our experimental findings on $CrCl_3$ at ν = 120 GHz and 240 GHz agree nicely with these reports and are detailed in Section 4.4.

2.4 Ginzburg-Landau Critical Model and Berezinskii-Kosterlitz-Thouless Model

The study of thermodynamic phase transitions plays an important role in understanding, describing, and predicting how transitions will arise and how various systems will behave. With a better understanding of these thermodynamic processes and laws, we are better able to illustrate and anticipate the behavior of a broad range of systems, including their inherent characteristics and how they may behave over time, in different conditions, or even in different dimensions. This deeper understanding of the phenomena we observe in a laboratory setting or on a daily basis is one of the most important roles in condensed matter and statistical physics. We can also say that one of the biggest ways that theoretical and experimental studies have driven the study of phase transitions is that we have gained a better understanding on how the lattice-dimensionality *d* and the spin-dimensionality *n* influence the critical behavior of many-body systems [48].

In recent years, and since the discovery of graphene, researchers have been seeking functional low-dimensional materials for use in next-generation devices due to their interesting

properties and tunability. Lower dimensions are desirable because it allows for new behaviors to arise, e.g. a change in magnetic or electronic correlations. Such materials may either be synthesized, as seen with the growth of thin films through epitaxy or similar methods, or mechanically exfoliated, as seen in many van der Waals magnets [49-51]. However, though we may find 2D materials very useful, describing 2D systems was not always so straightforward. According to the Mermin-Wagner theorem, continuous symmetries cannot be spontaneously broken at finite temperatures in systems with short-range interactions when $d \leq 2$ [22], meaning that phase transitions should not occur at or below the 2D limit. More specifically, this means that the 2D Heisenberg model does not order any finite temperature, making the Heisenberg model insufficient in describing 2D behavior. Luckily, there are a few other models that can be used to describe phase transitions at lower dimensions.

The *XY* model is a vector spin model that is better able to describe low-dimensional phase transitions and is able to adequately describe phase transitions involving spin vortices, a type of topological defect. Details of this model are seen in **Figure 2.4**. This model differs from the Heisenberg and Ising models in that there is, in a sense, no transition to long-range order, though there still exists a finite temperature where the magnetic susceptibility diverges [48]. This inability to possess a typical second-order phase transition arises, in part, from the presence of these spin vortices, which causes the system to be in a constant state of disorder and asymmetry. As mentioned earlier, the 2D Heisenberg spin model did not give a clear picture of transitions that take place when $d \leq 2$, but with the *XY* model it became possible to sufficiently describe the low-temperature phase transition that was seen when together Kosterlitz and Thouless, and independently Berezinskii, concluded that a topological phase transition due to the binding and

unbinding of magnetic vortices took place at the transition temperature of $T_{BKT} \neq 0$, known as the BKT transition, or often times the KT transition [43-45].

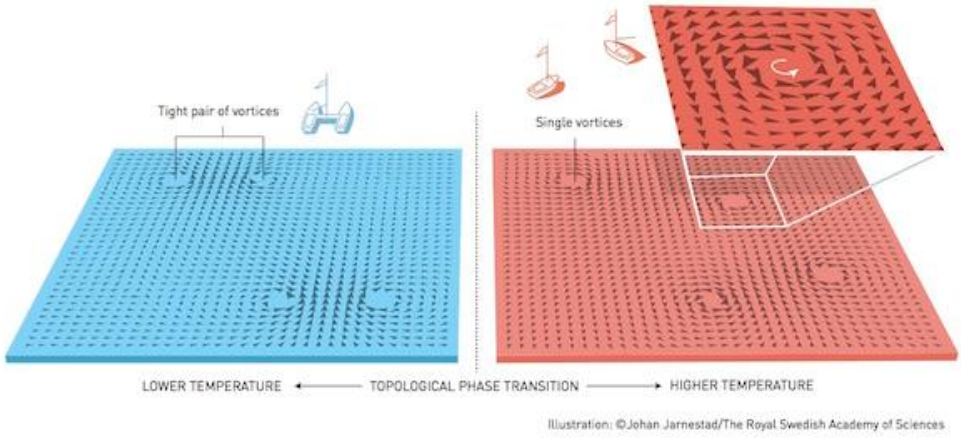

Figure 2.4: Spin vortices are not bound to each other at higher temperatures, and below T_{BKT} they become bound. This is the BKT transition.

This model is useful in that it allows for the proper description of low *d* systems approximated by the *XY* model and has previously been observed in thin films such as ultrathin ^{4}He superfluid films and various superconducting films [52,53], as well as in Josephson junctions [23]. Though this is model has been helpful in the field of condensed matter physics, there are still new discoveries surrounding this transition taking place. For instance, though this transition was previously understood to be unique to the 2D *XY* model and is not typically observed in condensed matter systems due to the presence of long-range order, which hampers the BKT transition [46], there have recently been a few studies suggesting that such systems can be adequately described by this phase transition [6-9,46,47]. Through the use of ESR spectroscopy, Ashoka *et al.* showed that the 3D manganite $Bi_{0.5}Sr_{0.5}Mn_{0.9}Cr_{0.1}O_3$ displayed 2D correlations by the BKT transition by showing that the angular dependence of the ESR linewidth is adequately described by the BKT model,

$$\Delta H(T) = \Delta H_{\infty} \exp\left[\frac{3b}{\sqrt{\left(\frac{T}{T_{BKT}}-1\right)}}\right] + mT + \Delta H_0 \qquad (2)$$

In our experiment, b has been set to $\pi/2$ for a square lattice in consistency with previous reports, although it has been shown to remain valid at any value [44]. The observed behavior can be attributed to an induced anisotropy by the applied magnetic field, as well as the presence of ferromagnetic and antiferromagnetic correlations within the sample, causing magnetic frustration within the 3D condensed matter system and causing it to effectively behave like a 2D system even in the absence of two-dimensionality. Here we see that there are traces of this unique transition in 3D condensed matter systems, or quasi-2D systems.

In addition to the BKT model described above, we also analyzed the temperature dependent ESR data for CrX_3 with the application of the Ginzburg-Landau critical model, which gives critical exponents that describe the dimensionality of a system. The critical model states,

$$\Delta H(T) = \frac{Q}{\left(\frac{T}{T_C}-1\right)^{p}} + mT + \Delta H_0 \qquad (1)$$

Here, Q is an arbitrary constant of proportionality, T_C is the Curie temperature or Néel temperature, and p is a critical exponent which is dependent on the spin and spatial degrees of freedom and can give a clear description of the dimensionality. The linear term m and a temperature independent term H are added to describe the physics far away from the magnetic phase transition [43,46] Using this model, we are able to describe the magnetic ordering of CrX_3 using p.

PART II: CHROMIUM TRIHALIDE CrX_3 (X = Cl, Br, I) ESR STUDIES

CHAPTER 3: $CRBR_3$ ESR STUDY

Among various van der Waals (vdW) magnets, CrX_3 (where X = Cl, Br, I) is a family of compounds that has gained considerable attention due to their cleavable nature and persistent magnetic properties even at the atomic limit [15,21,22-24]. Of these, $CrBr_3$ is a soft out-of-plane ferromagnetic insulator with a Curie temperature (T_C) of about 33 K [24,36] and has been reported to show spontaneous magnetization down to the monolayer [37]. It is an interesting platform to study magnetic interactions as atomically thin $CrBr_3$ has been shown to exhibit ferromagnetic interlayer coupling [40], while recent spin-polarized scanning tunneling microscopy and spectroscopy studies have confirmed this coupling to either be ferromagnetic (FM) or antiferromagnetic (AFM) in the bilayer depending on the stacking order [21]. Basic magnetic properties of this compound have been reported earlier [38,39] with the magnetism arising from the Cr^{3+} ion (S = 3/2, spin-only contribution) and the easy axis of magnetization along the *c*-axis.

$CrBr_3$ single crystals of dimension 1 x 1 mm were grown by the chemical vapor transport method as previously reported (See Ref. 17, 18), which is described in Section 2.1. High frequency ESR measurements were conducted at the National High Magnetic Field Laboratory located at Florida State University using the quasioptical spectrometer developed on-site. This system uses a superheterodyne spectrometer, employing a quasioptical submillimeter bridge that operates in reflection mode without cavity using a sweepable 17 T superconducting magnet [4,16]. In order to conduct ESR measurements as a function of angle θ (degrees) at T = 200 and 4 K, the sample was loaded into the instrument while attached to a sample rotator, allowing the plate-like sample to be rotated along the *c*-axis during ESR measurements. The $CrBr_3$ unit cell and atomic structure of the monolayer are shown in **Figure 2.2** in Section 2.2. The sample was cooled from room

temperature down to 200 K before a magnetic field was applied in order to ensure that the vacuum grease used to attach the sample to the rotator is solidified. ESR measurements were performed at ν = 240 GHz as a function of θ at both T = 200 K (paramagnetic phase) and 4 K (ferromagnetic phase) while the plate-like sample was rotated. Measurements were also conducted while the sample was held at a fixed angle of θ = 70°, due to an apparent field minimum at that angle, at the temperature range of T = 200 – 4 K (as shown in **Figure 3.1**). Magnetic susceptibility measurements were performed by employing a Quantum Design MPMS-3 SQUID magnetometer using a DC method [17,18].

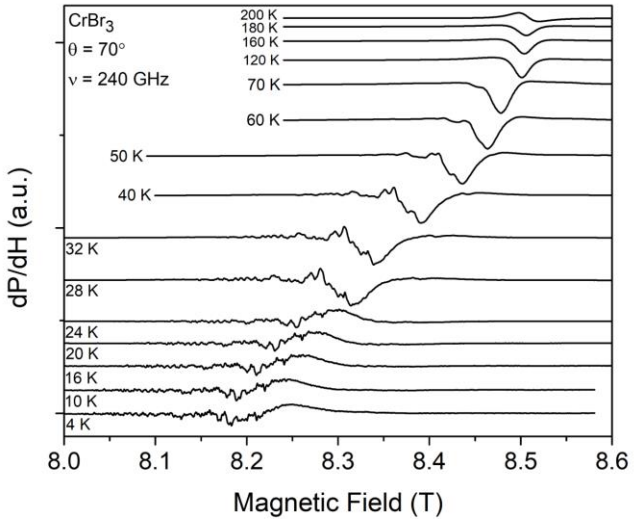

Figure 3.1: ESR signals as a function of temperature for $CrBr_3$ at a single fixed angle.

Figure 3.1 shows the 240 GHz ESR spectra collected at the fixed angle of θ = 70° over the temperature range of 200 – 4 K in order to gain insight into the behavior of the linewidth (full width at half maximum, ΔH) and resonance field. It is observed that the single paramagnetic signal of Lorentzian line shape at 200 K with g = 2.016 begins to split into multiple signals as the sample is cooled from 200 – 4 K. The temperature at which the single signal becomes multiple is in the vicinity of T_C = 33 K. Below T = 32 K down to 4 K, multiple signals arise, and the paramagnetic

signal broadens. Due to the high sensitivity of ESR spectroscopy, compared to conventional magnetometers, this technique is able to pick up ferromagnetic correlations even at $T >> T_C$ as reflected through the appearance of multiple signals at $T > 32$ K, consistent with previous reports [1-3]. Numerous ESR signals, as is seen in this experiment, are typically observed in ferromagnetic compounds due to magnetocrystalline anisotropy, magnetic inhomogeneity, and magnetic phase separation [54-59]. It is also worth noting that the spectroscopic *g*-value is seen to increase at a somewhat exponential rate as temperature is lowered from $T = 200 – 4$ K (not shown). At $T = 200$ K, $g = 2.016$ and at $T = 4$ K, $g = 2.082$. This g-value is within close proximity to $g = 2$ and is indicative of a quenched orbital moment that is typically seen in the Cr^{3+} ion [6,7]. This exponential behavior begins at $T = 40$ K, within close proximity to T_C, suggesting that this sharp change in *g*-value can be attributed to the creation of internal magnetic correlations as the temperature approaches the magnetic phase transition from above.

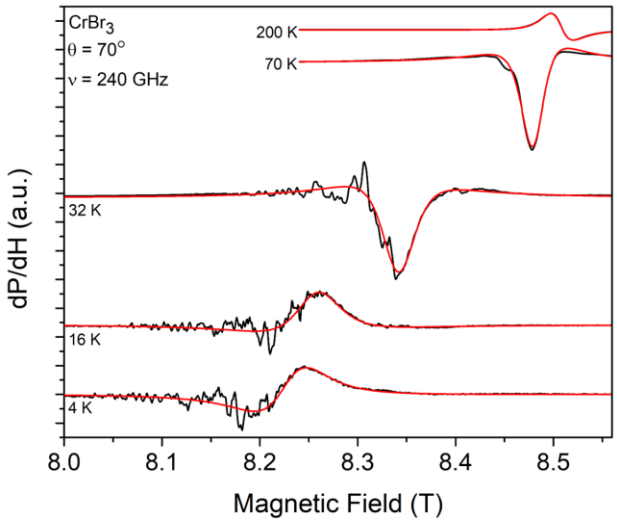

Figure 3.2: Computer-generated fits employing a Lorentzian line shape over a range of temperatures represented by the smooth red curve. The black curve is the ESR spectra collected on $CrBr_3$.

3.1 Ginzburg-Landau Critical Model and BKT Transition

The ESR spectral parameters were extracted using a Lorentzian fit at each temperature in the paramagnetic phase (40 – 200 K), some of which are shown in **Figure 3.2**. It should be noted that the narrow ESR signals modulated by a broader signal for the spectra measured at and below the magnetic phase transition were not fitted due to their apparent complexity. We first discuss the temperature dependence of the ESR linewidth as plotted in **Figure 3.3**. **Figure 3.3** shows the variation of linewidth as a function of temperature represented by solid squares, where the superimposed red curve is the computer-generated fit resulting from the Ginzburg-Landau critical model, which states,

$$\Delta H(T) = \frac{Q}{\left(\frac{T}{T_C}-1\right)^{p}} + mT + \Delta H_0 \qquad (1)$$

Details of the Ginzburg-Landau critical model can be found in Section 2.4. **Figure 3.3** also shows the variation of linewidth as a function of temperature along with the fit generated using the BKT model, a phase transition that takes place at finite temperatures previously understood to be unique to the 2D *XY* model, a limiting case of the 2D Heisenberg model [24]. A transition of this type is not usually observed in condensed matter systems due to inherent interlayer coupling which inhibits the BKT transition due to long-range order [46], a property that 2D Heisenberg magnets lack at finite temperatures [22]. The BKT transition, which is typically found in 2D systems approximated by the *XY* model asserts,

$$\Delta H(T) = \Delta H_\infty \exp\left[\frac{3b}{\sqrt{\left(\frac{T}{T_{BKT}}-1\right)}}\right] + mT + \Delta H_0 \qquad (2)$$

Details on the BKT model are outlined in Section 2.4. **Figure 3.3** illustrates that our obtained ESR data is described very nicely by (1) and (2) in the region well above the magnetic

phase transition (see **Table 1** for extracted fit parameters), with the extrapolated critical exponent $p = 0.9$. This is very close to the reported value of $p = 0.5 – 0.7$, which has been reported in most of the previously investigated layer-type antiferromagnets studied by Benner and Boucher [60]. Similar values of $p = 0.78$ and 0.85 have also been reported in $HCrO_2$ and $NaCrO_2$ respectively and are suggestive of antiferromagnetic fluctuations [6]. A similar BKT-like transition has been observed in the Cr^{3+}-doped three-dimensional (3D) magnets such as $Bi_{0.5}Sr_{0.5}Mn_{0.9}Cr_{0.1}O_3$ by Ashoka and co-authors [46,47]. Through the temperature dependence of the ESR linewidth, the authors employed the BKT model to satisfactorily describe their experimental findings. The authors explained this observation in terms of an effective 2D *XY* easy plane anisotropy induced by the magnetic field applied in the ESR experiment that presumably induces an interaction between the long-range spin vortices and spin clusters that may have been formed during magnetic phase segregation [46]. In a separate study, these authors tested the hypothesis that the applied EPR field is responsible for the onset of BKT-like behavior in $BaNi_2V_2O_8$ and have shown that a higher applied field allows for a higher temperature onset of the threshold anisotropy required for BKT behavior which will manifest as a higher T_{BKT} [47]. This behavior is evidenced in another work, where Seehra and co-authors find that the ESR linewidth in $CrBr_3$ behaves differently when the frequency is increased from 9.1 GHz to 24 GHz [11]. As the applied field increases, the thermal behavior of the linewidth and correlation length around T_C begins to vary, where the spectroscopic linewidth broadens from $\Delta H \sim 55$ Oe at $\nu = 9.1$ GHz to $\Delta H \sim 65$ Oe at $\nu = 24$ GHz. This is in good agreement with our data at $\nu = 240$ GHz, where the linewidth is calculated to be $\Delta H = 670$ Oe at $T = 32$ K (not shown).

Here, we will try to understand how bulk $CrBr_3$ may exhibit magnetic phase separation, which has traditionally been known as a single phase ferromagnet [23,24,38,39]. Quite

interestingly, in a recent report using Raman spectroscopy mapping, Li and co-authors [61] revealed a novel mixed state of layered antiferromagnetism and ferromagnetism in 3D CrI_3 bulk crystals where the layered antiferromagnetism survives in the surface layers and the ferromagnetism appears in deeper bulk layers. Due to the structural similarities between CrI_3 and the title compound, $CrBr_3$ is also expected to exhibit magnetic phase separation (**Figure 3.6**), and with the applicability of BKT model on $CrBr_3$ demonstrated, we have shown that there is ample evidence of 2D correlations present within layered $CrBr_3$. This is argued to be caused by the presence of both FM and AFM correlations within a single bulk sample, as well as a consequence of the spectrometer's applied magnetic field combined with the inherent anisotropy in $CrBr_3$ [21,42-44,61]. This point is also substantiated by Kalenyuk *et al.*, where the authors report that the dimensionality can be tuned by varying the temperature as well as the magnetic field, even in the non-layered low anisotropic materials [62]. Signatures of field induced BKT 2D correlations have also been observed in many compounds as reported in the past [46,47,63]. Furthermore, it has been theoretically predicted some time ago that an applied magnetic field is able to induce 2-dimensionality [64].

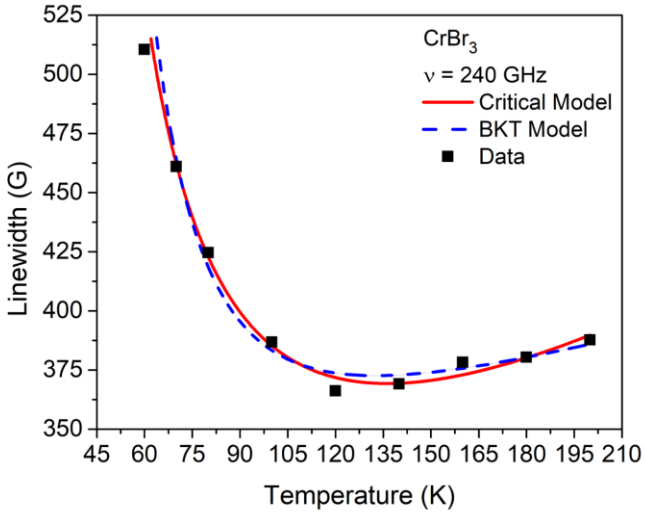

Figure 3.3: Temperature dependence of the ESR linewidth collected on $CrBr_3$ at the fixed angle $\theta = 70°$; fitted to the Ginzburg-Landau critical model (solid red line) and Berezinskii-Kosterlitz-Thouless model (dashed blue line).

Table 3.1: Values of fit parameters and goodness of fit obtained from the Ginzburg-Landau critical model and BKT model on $CrBr_3$.

Critical model		BKT model	
Exponent From Fit		Exponent From Fit	
Q (T)	294.1	H (T)	117.5
p	0.9043	T_{BKT} (K)	13.74
T_C (K)	32	b	$\pi/2$
m (T/K)	0.8759	H_∞ (T)	27.64
H (T)	148.9	m (T/K)	0.8641
R^2	0.9903	R^2	0.9906

3.2 Angular Dependence of the Resonance Field

We now focus on the angular dependence of the ESR resonance field and linewidth. In **Figure 3.4(a)**, we have plotted the resonance field (solid squares, left y-axis) as well as the *g*-value (hollow inverted triangles, right y-axis) as a function of angle collected at $T = 200$ K. The *g*-values were interpolated with a spline function. The angular dependence of the resonance field is fitted with the model,

$$\mathrm{H_{res}}(\theta) = \mathrm{F}(3\cos^2\theta - 1) + \mathrm{G} \qquad (3)$$

The observed $(3cos^2\theta - 1)$-like behavior of the resonance field is a characteristic behavior of 2D magnetic systems [13,65] and has earlier been observed in K_2MnF, K_2CuF, as well as $CrCl_3$, which has been experimentally shown to exhibit 2D Heisenberg behavior and is reported to have correlations suggestive of a weak *XY* model [13,42,61]. The curve connecting the resonance field

values results from the fit using (3). An identical trend is observed for the angular dependence of resonance field and *g*-value when the measurement is conducted at T = 4 K, as plotted in **Figure 3.4(b)**. This marked angular dependence of the resonance field at both temperatures has been described as the noncubic distribution of the dipoles within the 2D lattice where the resulting net dipolar field shifts the resonance field according to (3) [13].

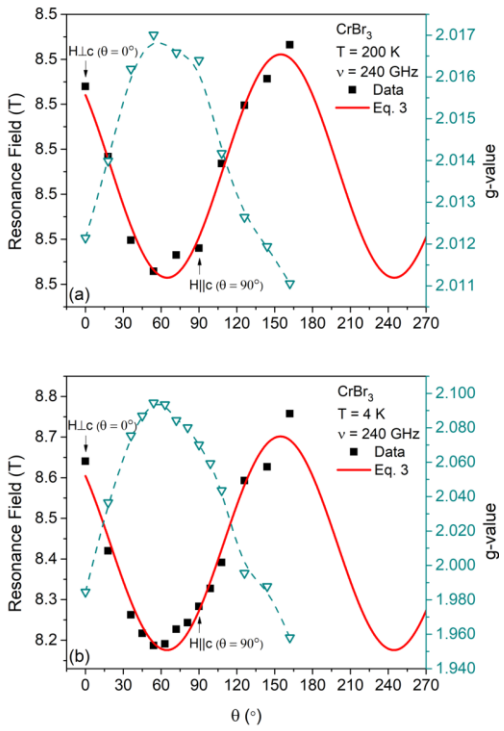

Figure 3.4: Angular dependence of the resonance field coming from $CrBr_3$ at: (a) 200 K and (b) 4 K fitted with a modified form of (3) to take into account a phase shift: $H_{res}(\theta) = F[3\cos^2(\theta - \phi) - 1] + G$. Here, the cyan data points show the calculated *g*-values with a B-spline to guide the eye and illustrate the inverse relationship between resonance field and *g*-value.

3.3 Angular Dependence of the Linewidth

Equation (4) accurately and adequately describes the dependence of the linewidth on θ, both in the ferromagnetic and paramagnetic phases as seen in **Figure 3.5**,

$$\Delta H(\theta) = A(3\cos^2\theta - 1)^2 + B \qquad (4)$$

The nearly "W"-shaped angular dependence of the linewidth observed here is unique to low-dimensional magnets and has been previously reported in $MnPS_3$, a compound that has been shown to have 2D characteristics [66], as well as other 2D magnetic systems such as the 2D antiferromagnet K_2MnF_4 [60] and the out-of-plane 2D Heisenberg antiferromagnet $CrCl_3$ [13], which, as mentioned previously, is closely related to $CrBr_3$ due to their structural similarities. The unique shape of this curve with a maximum near lower angles, and a shallow minimum near θ = 55°, or the "magic" angle, has been observed in other systems and is a known feature of low-dimensional systems [60]. Similar to the model described by (3), this $(3\cos^2\theta - 1)^2$-like behavior is also characteristic of 2D magnetic systems [13].

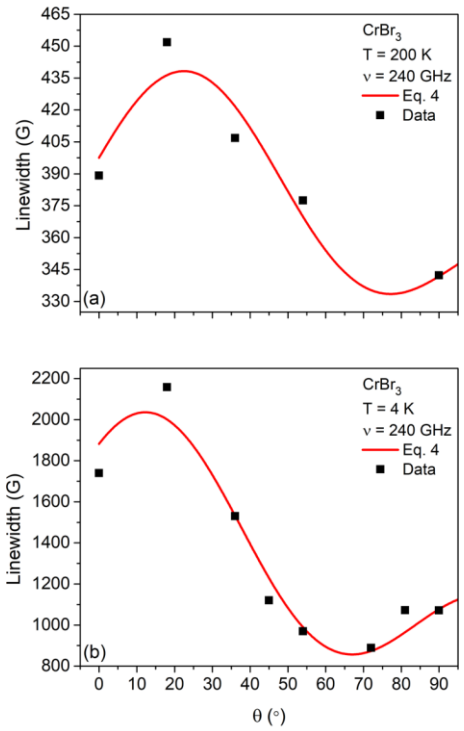

Figure 3.5: Angular dependence of the linewidth coming from $CrBr_3$ at: (a) 200 K and (b) 4 K fitted with a modified form of (4) to take into account a phase shift: $\Delta H(\theta) = A[3\cos^2(\theta - \phi) - 1]^2 + B$.

3.4 Magnetization

In addition to ESR measurements, temperature dependent magnetization measurements were conducted upon zero-field- and field-cooled (ZFC and FC) conditions from $T = 2 – 300$ K in order to gain insight into the magnetic correlations. In a recent report using Raman spectroscopy mapping, Li and co-authors [61] revealed a novel mixed state of layered antiferromagnetism and ferromagnetism in 3D CrI_3 bulk crystals where the layered antiferromagnetism survives in the surface layers and the ferromagnetism appears in deeper bulk layers. Due to the structural similarities between CrI_3 and the title compound, one may expect that the latter will also exhibit magnetic phase separation. For FC measurements, a magnetic field of $H = 0.01$ T was applied along the *c*-axis (easy axis) while cooling the sample. As shown in **Figure 3.6**, a clear bifurcation between ZFC and FC traces is observed below T_C (see supplementary information, Ref. 18). This single-crystalline $CrBr_3$ sample is well characterized and has been used in previous studies [17,18] and is therefore expected to contain minimal crystal defects and crystal grains, suggesting that this splitting is an indicator of a possible competing minute magnetic phase present along with the dominant ferromagnetic phase. Similar splitting between the ZFC and FC curves has been reported previously in a number of low dimensional magnets such as $CeCrO_3$, $Pr_{0.5}Sr_{0.5}MnO_3$, and the nanoscale charge ordered (CO) manganites $RE_{1-x}AE_xMnO_3$ (RE = Nd, Pr; AE = Ca; x = 0.5). [54,67,68] However, as discussed below, we did not observe strong evidence of possible magnetic phase separation that may warrant the applicability of BKT model in $CrBr_3$. Firstly, in analyzing the molar magnetic susceptibility χ_{mol}, we have calculated a Curie-Weiss (CW) temperature of θ_{CW} = 50.53 K by fitting with the CW expression $\chi - \chi_0 = C/(T - \theta_{CW})$, where C is the CW constant and χ_0 is a small background. While the frustration index [18] $f = \theta_{CW}/T_C$ is finite (> 1), its magnitude is relatively smaller. Secondly, to our knowledge, one report [69] appeared in the

literature where the authors infer the indications of BKT behavior through the temperature dependence of susceptibility collected when the ideal 2D frustrated magnet $TmMgGaO_4$ is cooled under various magnetic field strengths. The authors observed that the susceptibility increases as the magnetic field decreases below $T < 2$ K (upper BKT transition), suggesting the onset of peculiar magnetic correlations. We did not see this behavior in our preliminary susceptibility measurements (**Figure 3.6**) on $CrBr_3$, in which the susceptibility increases as the cooling field increases. That might suggest that BKT phase does not exist in $CrBr_3$. Therefore, we rule out the possible presence of BKT phase/correlations in $CrBr_3$. However, additional work is required to further the understanding.

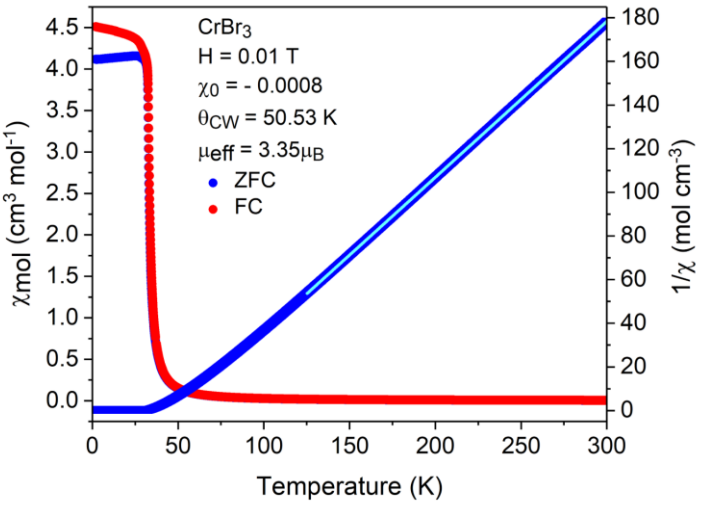

Figure 3.6: Temperature dependence of magnetic susceptibility under zero-field- and field-cooled conditions show a pronounced bifurcation between ZFC (blue) and FC (red) curves (left y-axis). Temperature dependence of the inverse susceptibility (blue curve, right y-axis) is fitted with the CW expression (cyan line) [see supplementary information, Ref. 18].

CHAPTER 4: $CRCL_3$ ESR STUDY

$CrCl_3$ is a layered van der Waals (vdW) material with a Néel temperature (T_N) of about 17 K [3]. Though $CrCl_3$ has been studied for many years, it has recently emerged as a promising candidate in the context of vdW magnets for use in next-generation spintronic devices due to its exceptional and tunable properties [3,5,32]. Although a member of the CrX_3 (where X = Cl, Br, I) family due to their similar structures and tunable magnetic properties, $CrCl_3$ is unique in that it is an in-plane ferromagnet and out-of-plane antiferromagnet. $CrCl_3$'s magnetic Cr^{3+} ions (S = 3/2) are in the center of the octahedral unit cell, where the edge-sharing octahedra form in the *ab* plane creating a honeycomb lattice [3].

In this study we perform ESR spectroscopy on plate-like $CrCl_3$ of dimension 2 x 3 mm at ν = 120 GHz as a function of temperature (T = 289 – 5 K) and separately at ν = 240 GHz as a function of angle of rotation θ (degrees) and temperature (T = 200 – 4.4 K) in order to study the magnetic interactions and dimensionality. **Figure 4.1(a)** shows the ESR spectra collected at ν = 120 GHz (T = 289 – 5 K) at a fixed, arbitrary angle, while **Figure 4.1(b)** shows the spectra collected at the fixed angle of θ = 0° at ν = 240 GHz (T = 200 – 4.4 K) in order analyze the behavior of the resonance field and linewidth (full width at half maximum, ΔH). Frequency dependent measurements were conducted at the National High Magnetic Field Laboratory located at Florida State University using the quasioptical spectrometer developed on-site. As with all CrX_3 compounds in this experiment, the sample was loaded into the instrument while attached to a sample rotator, allowing the plate-like sample to be rotated during ESR measurement [16].

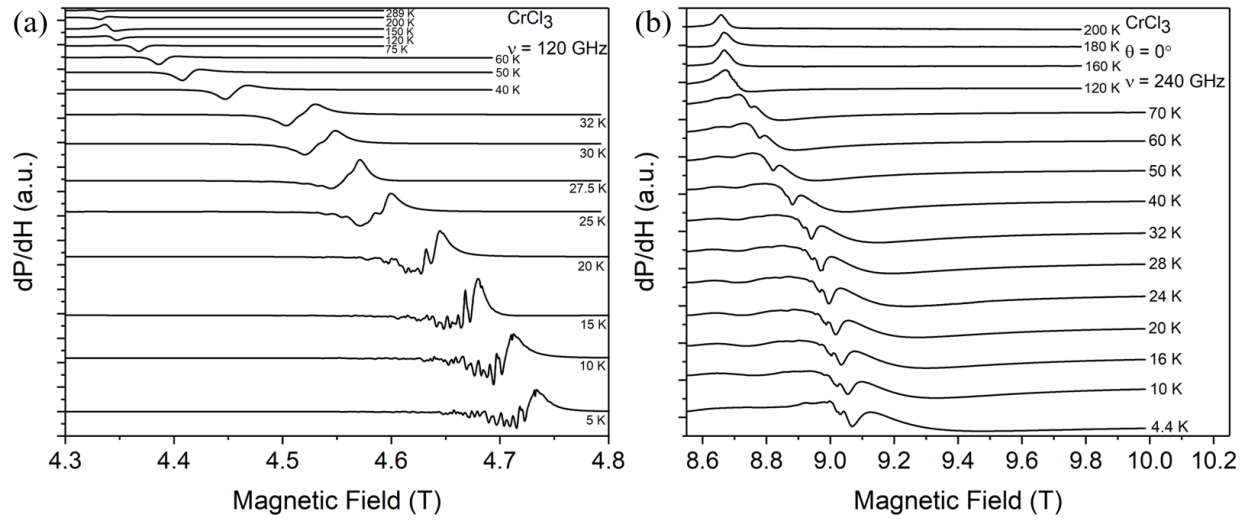

Figure 4.1: ESR signals as a function of temperature for $CrCl_3$ at (a) v = 120 GHz, T = 289 – 5 K and (b) v = 240 GHz, T = 200 – 4.4 K.

The ESR spectra collected from $CrCl_3$ at the two frequencies, v = 120 GHz and 240 GHz, are shown in **Figure 4.1**. The single paramagnetic signals of Lorentzian line shape at higher temperatures are seen to become multiple as the temperature is lowered and approaches T_N = 17 K (fits employing a Lorentzian line shape can be seen in **Figure 4.2**). This happens much earlier at $T \sim 70$ K in the 240 GHz experiment versus $T \sim 32$ K in the 120 GHz experiment, highlighting the increased sensitivity when ESR spectroscopy is performed at higher frequencies. As mentioned in Chapter 3, this ability to detect magnetic behavior above T_N is due to the high sensitivity of ESR spectroscopy which is able to pick up magnetic correlations even at $T >> T_N$, as reflected through the appearance of multiple signals above T_N and is also seen in our $CrBr_3$ experiment conducted at 240 GHz. ΔH typically linearly decreases when the temperature approaches T_N from above due to the motionally narrowed relaxation in a system with ferromagnetic clusters or magnetic polarons. However, the broadening effect of ΔH caused by the tendency of the enhanced exchange

interaction among ferromagnetic clusters or the enhancement of magnetic inhomogeneity can also be developed due to the creation of internal magnetic fields with decreasing temperature [16,70], such as the one observed in the present work on $CrCl_3$ and $CrBr_3$.

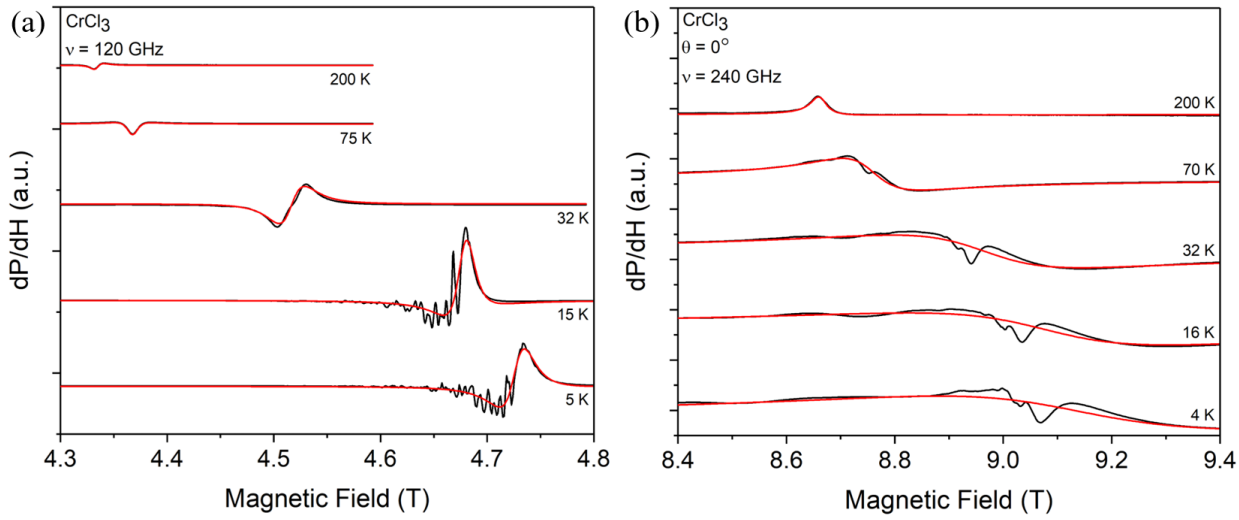

Figure 4.2: Computer generated fits employing a Lorentzian line shape over a range of temperatures represented by the smooth red curve. Black curves are the ESR spectra collected from $CrCl_3$ experiments performed at (a) $\nu = 120$ GHz and (b) $\nu = 240$ GHz.

4.1 Ginzburg-Landau Critical Model and BKT Transition

Here we will discuss the temperature dependence of the ESR linewidth when conducted on single crystalline $CrCl_3$ at $\nu = 240$ GHz, as plotted in **Figure 4.3**. The figure shows the change in linewidth as a function of temperature as represented by the black squares fitted to the Ginzburg-Landau critical model represented by the red curve. The critical model states,

$$\Delta H(T) = \frac{Q}{\left(\frac{T}{T_C} - 1\right)^{p}} + mT + \Delta H_0 \qquad (1)$$

Details on Eq. 1 are discussed in detail in Section 2.4. We also fit the BKT transition model to the temperature dependence of the ESR linewidth, as represented by the dashed blue line in **Figure**

4.3. The BKT transition is a phase transition that takes place at finite temperatures previously understood to be unique to the 2D *XY* model, a limiting case of the 2D Heisenberg model [24]. As mentioned in previous chapters, a transition of this type is not usually observed in condensed matter systems of this type due to inherent interlayer coupling which inhibits the BKT transition due to long-range order [46], a property that 2D Heisenberg magnets lack at finite temperatures [22] and is typically found in 2D systems approximated by the *XY* model. The BKT model states,

$$\Delta H(T) = \Delta H_{\infty} \exp\left[\frac{3b}{\sqrt{\left(\frac{T}{T_{BKT}}-1\right)}}\right] + mT + \Delta H_0 \qquad (2)$$

Details on the BKT model can also be found in Section 2.4. **Figure 4.3** shows that the temperature dependence of the ESR linewidth in $CrCl_3$ is described nicely by (1) and (2) in the paramagnetic region above T_N. In analyzing the critical exponent p, which describes the dimensionality of the system, we find that $p = 0.2888$ (**Table 4.1**). This is much lower than what was calculated for $CrBr_3$ and falls below the two regions discussed in Chapter 3. In previous reports, $p = 0.5 – 0.7$ and $p = 0.78 – 0.85$ were reported in layer-type antiferromagnets studied by Benner and Boucher [60], and in $HCrO_2$ and $NaCrO_2$ which exhibits antiferromagnetic fluctuations [6], respectively. However, when the critical model is fitted to the variation of the linewidth as a function of temperature in the $\nu = 120$ GHz experiment, a critical exponent of $p = 0.8235$ is extrapolated, a value indicative of antiferromagnetic fluctuations in $CrCl_3$ [6,60]. While the fits performed on both sets of data are considered good fits as indicated by their goodness of fit values (R^2), it should be noted that $R^2 = 0.9994$ at 240 GHz and $R^2 = 1$ at 120 GHz. This suggests a better fit on the 120 GHz data and suggests that $p = 0.8$ is more precise. The BKT and critical model fits on the $\nu = 120$ GHz experiment will be discussed in Section 4.4.

As mentioned in Section 3.1, a similar BKT-like transition has been observed in the Cr^{3+}-doped three-dimensional (3D) magnet $Bi_{0.5}Sr_{0.5}Mn_{0.9}Cr_{0.1}O_3$ by Ashoka *et al.* [46]. Through the temperature dependence of the ESR linewidth, the authors employed the BKT model to satisfactorily describe their experimental findings. This observation is explained in terms of an effective 2D *XY* easy plane anisotropy induced by the magnetic field applied in the ESR experiment that presumably induces an interaction between the long-range spin vortices and spin clusters that may have been formed during magnetic phase segregation [46]. In a separate study, these authors tested the hypothesis that the applied EPR field is responsible for the onset of BKT-like behavior in $BaNi_2V_2O_8$ and have shown that a higher applied field allows for a higher temperature onset of the threshold anisotropy required for BKT behavior which will manifest as a higher BKT transition temperature, T_{BKT} [47]. This behavior is evidenced in another work, where Seehra and co-authors find that the ESR linewidth in $CrBr_3$ behaves differently when the frequency used in the ESR experiment is increased from 9.1 GHz to 24 GHz [11]. As mentioned, we have conducted ESR spectroscopy at 120 and 240 GHz and noticed both an increase in T_{BKT} and linewidth as the applied field is increased. Details of these experiments are discussed below in Section 4.4.

We believe that the critical exponent *p* and the BKT transition model accurately describe the behavior in $CrCl_3$ and can attribute this behavior to the fact that the compound is an in-plane ferromagnet and out-of-plane antiferromagnet, suggesting magnetic frustration within the system. Though due to the lack of magnetic separation in $CrCl_3$, the BKT model in not necessarily applicable. It is important, however, to note that $CrCl_3$ has been reported to exhibit 2D Heisenberg behavior and is reported to have correlations suggestive of a weak *XY* model, a model favored by the BKT transition [13,42,61]. In a recent report using Raman spectroscopy mapping, Li and co-

authors [61] revealed a novel mixed state of layered antiferromagnetism and ferromagnetism in 3D CrI_3 bulk crystals where the layered antiferromagnetism survives in the surface layers and the ferromagnetism appears in deeper bulk layers. Due to the structural similarities in CrX_3, $CrCl_3$ is also expected to exhibit magnetic phase separation, and with the applicability of BKT model on $CrCl_3$ demonstrated, we have shown that there is ample evidence of 2D correlations present within the compound. This is argued to be caused by the presence of both FM and AFM correlations within a single bulk sample, as well as a consequence of the spectrometer's applied magnetic field combined with the inherent anisotropy in $CrCl_3$ [21,42-44,61]. This point is also substantiated by Kalenyuk *et al.*, where the authors report that the dimensionality can be tuned by varying the temperature as well as the magnetic field, even in the non-layered low anisotropic materials [62]. Signatures of field induced BKT 2D correlations have also been observed in many compounds as reported in the past [46,47,63]. Furthermore, it has been theoretically predicted some time ago that an applied magnetic field is able to induce 2-dimensionality [64].

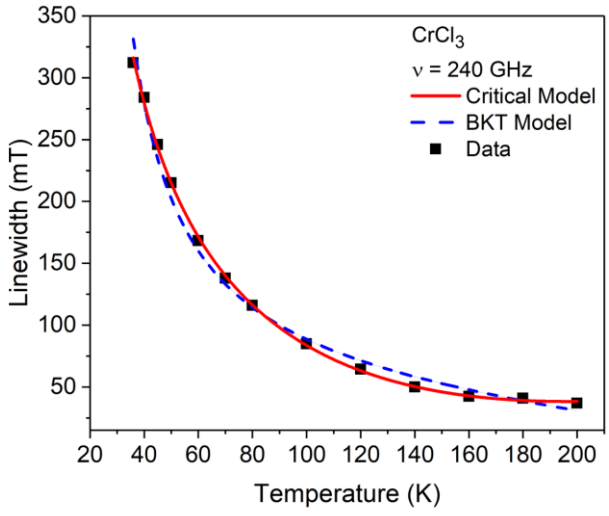

Figure 4.3: Temperature dependence of the ESR linewidth on $CrCl_3$ at a fixed angle of $\theta = 0°$ conducted at $\nu = 240$ GHz; fitted to the Ginzburg-Landau critical model (solid red line) and Berezinskii-Kosterlitz-Thouless model (dashed blue line).

Table 4.1: Values of fit parameters and goodness of fit obtained from the Ginzburg-Landau critical model and BKT model on $CrCl_3$ at v = 240 GHz.

Critical model		BKT model	
Exponent From Fit		Exponent From Fit	
Q (T)	838.6	H (T)	0.3024
p	0.2888	T_{BKT} (K)	8.094
T_C (K)	17	b	π/2
m (T/K)	0.6178	H_∞ (T)	26.72
H (T)	-508.7	m (T/K)	-0.199
R^2	0.9999	R^2	0.9915

4.2 Angular Dependence of the Resonance Field

We now focus on the angular dependence of the ESR resonance field collected on $CrCl_3$ at v = 240 GHz. In **Figure 4.4(a)**, we have plotted the resonance field (solid squares, left y-axis) as well as the g-value (hollow inverted triangles, right y-axis) as a function of angle collected at T = 200 K. The g-values were interpolated with a spline function. The angular dependence of the resonance field is fitted with Eq. 3. The observed $(3cos^2\theta - 1)$-like behavior of the resonance field is a characteristic behavior of 2D magnetic systems [13,65] and has earlier been observed in K_2MnF, K_2CuF, as well as $CrCl_3$, which has been experimentally shown to exhibit 2D Heisenberg behavior and is reported to have correlations suggestive of a weak XY model [13,43,61]. The curve connecting the resonance field values results from the fit using (3). An identical trend is observed for the angular dependence of resonance field and g-value when the measurement is conducted at T = 4 K, as plotted in **Figure 4.4(b)**. This marked angular dependence of the resonance field at

both temperatures has been described as the noncubic distribution of the dipoles within the 2D lattice where the resulting net dipolar field shifts the resonance field according to (3) [13].

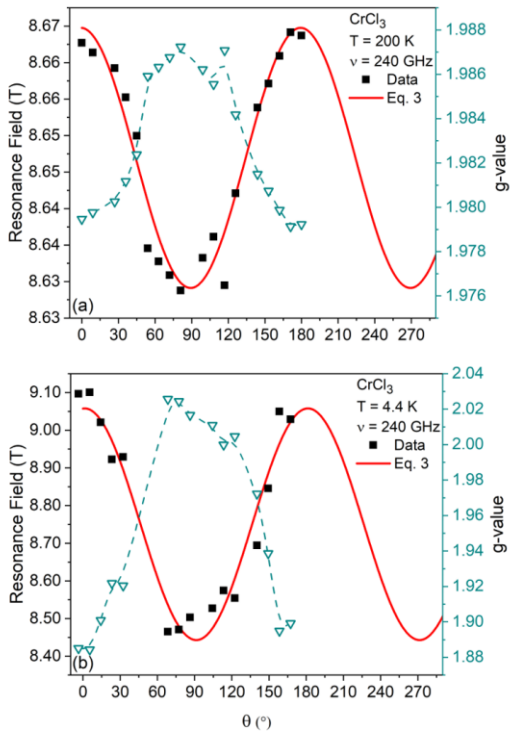

Figure 4.4: Angular dependence of the resonance field of $CrCl_3$ at: (a) 200 K and (b) 4.4 K fitted with a modified form of (3) to take into account a phase shift: $H_{res}(\theta) = F[3\cos^2(\theta - \phi) - 1] + G$. Here, the cyan data points show the calculated *g*-values with a B-spline to guide the eye and illustrate the inverse relationship between resonance field and *g*-value.

4.3 Angular Dependence of the Linewidth

We find that Eq. 4 accurately and adequately describes the dependence of the linewidth on θ, both in the ferromagnetic and paramagnetic phases as seen in **Figure 4.5**. The nearly "W"-shaped angular dependence of the linewidth observed here is unique to low-dimensional magnets and has been previously reported in $MnPS_3$, a compound that has been shown to have 2D characteristics [66], as well as other 2D magnetic systems such as the 2D antiferromagnet K_2MnF_4 [60] and the out-of-plane 2D Heisenberg antiferromagnet $CrCl_3$ [13]. The unique shape of this

curve with a maximum near lower angles, and a shallow minimum near θ = 55°, or the "magic" angle, has been observed in other systems and is a known feature of low-dimensional systems [60]. Similar to the model described by (3), this $(3\cos^2\theta - 1)^2$-like behavior is also characteristic of 2D magnetic systems [13].

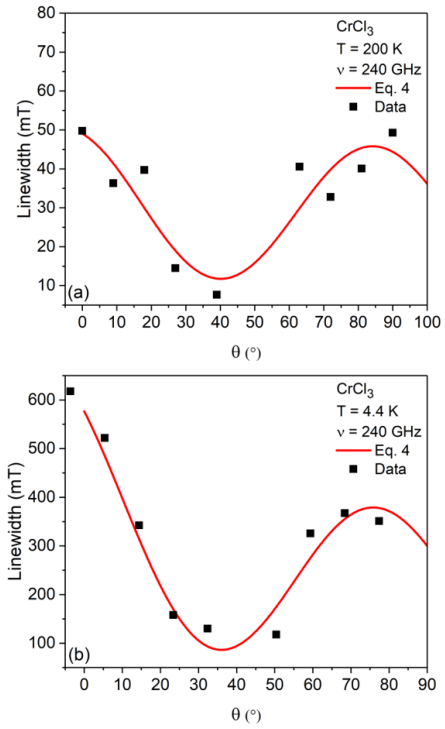

Figure 4.5: Angular dependence of the linewidth collected from $CrCl_3$ at: (a) 200 K and (b) 4.4 K fitted with a modified form of (4) to take into account a phase shift: $\Delta H(\theta) = A[3\cos^2(\theta - \phi) - 1]^2 + B$.

4.4 Frequency Dependence of the ESR Linewidth

When conducting ESR spectroscopy as a function of temperature at different frequencies on $CrCl_3$, we notice that the signals shift toward higher fields in both ν = 120 GHz and ν = 240 GHz experiments, as seen in **Figure 4.1**. However, when measured at ν = 240 GHz we see the onset of ferromagnetic correlations, as mentioned in Chapter 3 in the case of $CrBr_3$, at a much higher temperatures than in the ν = 120 GHz experiment. At ν = 120 GHz, ferromagnetic

correlations begin to appear at around $T \sim 32$ K, while at $\nu = 240$ GHz they appear much sooner at temperatures as high as ~ 70 K due to the appearance of multiple signals in those ranges, demonstrating the increased sensitivity of ESR conducted at higher frequencies. The ESR linewidth is also seen to increase in $CrCl_3$ when the frequency is increased, in good agreement with the work done by Seehra *et al.*, where the authors observed that the ESR linewidth increases with an increased applied field in $CrBr_3$ [11]. When ESR was conducted at $\nu = 120$ GHz: at $T = 200$ K, $\Delta H = 150.393$ Oe and at $T = 5$ K, $\Delta H = 387.983$ Oe. In the $\nu = 240$ GHz experiment: at $T = 200$ K, $\Delta H = 367.59$ Oe and at $T = 4.4$ K, $\Delta H = 6{,}172.72$ Oe.

Another consequence of the spectrometers increased applied field in an increase in the BKT temperature. According to Ashoka *et al.*, a higher applied magnetic field allows for a higher temperature onset of the threshold anisotropy required for BKT-like behavior, which will cause an increase the onset BKT temperature, T_{BKT} [47]. In this frequency dependent study on $CrCl_3$, the linewidth and resonance field from 120 GHz and 240 GHz experiments were also fitted using Eq. 2 and show that T_{BKT} increases from $T_{BKT} = 6.758$ K @ 120 GHz to $T_{BKT} = 8.094$ K @ 240 GHz. The BKT and critical model fits on the variation to the linewidth as a function of temperature for both experiments can be seen in **Figure 4.3** and **Figure 4.6**, and a detailed comparison of the parameters extracted from these fits can be seen in **Table 4.2**.

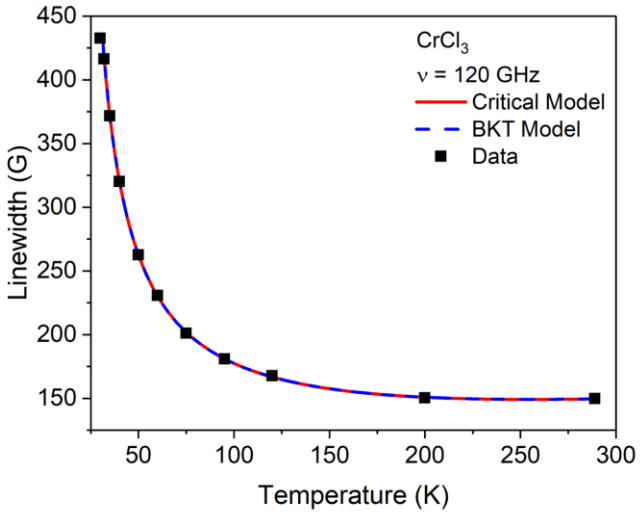

Figure 4.6: Temperature dependence of the ESR linewidth on $CrCl_3$ conducted at ν = 120 GHz; fitted to the Ginzburg-Landau critical model (solid red line) and Berezinskii-Kosterlitz-Thouless model (dashed blue line).

Table 4.2: Values of fit parameters and goodness of fit obtained from the Ginzburg-Landau critical model and BKT model on $CrCl_3$ experiments performed at ν = 120 GHz and ν = 240 GHz.

Critical model			BKT model		
Exponent From Fit	**120 GHz**	**240 GHz**	Exponent From Fit	**120 GHz**	**240 GHz**
Q (T)	249.9	2,397	H (T)	57.87	0.3024
p	0.8235	0.2888	T_{BKT} (K)	6.7575	8.094
T_C (K)	17	17	b	π/2	π/2
m (T/K)	0.1168	0.9739	H_∞ (T)	31.01	26.72
H (T)	85.85	-2,092	m (T/K)	0.098384	-0.199
R^2	1	0.9994	R^2	0.9999	0.9915

CHAPTER 5: ONGOING CRI_3 ESR STUDY

Interest in CrI_3 was recently rejuvenated when long-range magnetic order in pristine two-dimensional (2D) crystals $Cr_2Ge_2Te_6$ and CrI_3 [14], as well as the discovery of 2D ferromagnetism in the CrI_3 monolayer were first reported [25], renewing interest in compounds with similar magnetic and structural properties. CrI_3 is an out-of-plane ferromagnet with persistent magnetic properties down to the monolayer and a Curie temperature (T_C) of 61 K [10,31,34,35]. However, it has also been shown to exhibit interlayer antiferromagnetism in the bilayer [21] making it an interesting candidate in this study where we attempt to track the system's magnetic frustration using ESR spectroscopy. The thin plate-like single crystal of CrI_3 of dimension 0.5 x 0.5 mm used in this study was grown via the chemical vapor transport (CVT) method as described in Refs. [19] and is discussed in Section 2.1. Additionally, all ESR experimental settings were kept constant for reproducibility. High frequency (ν = 240 GHz) ESR measurements were recorded at the National High Magnetic Field Laboratory located at Florida State University using the quasioptical spectrometer developed on-site. This setup uses a superheterodyne spectrometer, employing a quasioptical submillimeter bridge that operates in reflection mode without cavity using a sweepable 17 T superconducting magnet [16]

To better understand the magnetic interactions, magnetic nature, and dimensionality of CrI_3, we have conducted ESR spectroscopy at ν = 240 GHz on bulk CrI_3 as a function of angle θ (degrees) at T = 200 and 4.4 K, and as a function of temperature from T = 200 – 4 K. As this study is ongoing, we will exclusively discuss the angular dependence of the linewidth (full width at half maximum, ΔH) and resonance field at T = 200 K. Similar to the $CrBr_3$ and $CrCl_3$ studies discussed in Chapters 3 and 4, we have fitted our ESR spectra with a Lorentzian line shape in order to analyze the spectral parameters such as linewidth, resonance field and spectroscopic g-value in order to gain insight on the local magnetic nature, magnetic phase transitions and magnetic interactions in CI_3.

While the ESR experiments are currently under investigation, here, we analyze the angular dependence of the resonance field and linewidth with Eq. 3 and Eq. 4 at T = 200 K as seen in **Figure 5.1**. In **Figure 5.1(a)**, we have plotted the resonance field (solid squares, left y-axis) as well as the g-value as a function of angle collected at T = 200 K. The g-values are plotted on the right y-axis, are indicated by the hollow inverted triangles, and were interpolated with a spline function to guide the eye. The angular dependence of the resonance field is fitted with Eq. 3. The observed $(3cos^2\theta - 1)$-like behavior of the resonance field is a characteristic behavior of 2D magnetic systems [13,65] and has earlier been observed in K_2MnF, K_2CuF, as well as $CrCl_3$, which has been experimentally shown to exhibit 2D Heisenberg behavior and is reported to have correlations suggestive of a weak XY model [13,42,61]. In **Figure 5.1(b)** we have plotted the angular dependence of the linewidth at T = 200 K and find that Eq. 4 describes the dependence of the linewidth on θ in the paramagnetic phase. In comparing the fit from Eq. 4 with the previous chapters, we see an even more clear "W"-shaped angular dependence of the linewidth which is unique to low-dimensional magnets. This characteristic behavior has been previously reported in $MnPS_3$, a compound that has been shown to have 2D characteristics [66], as well as other 2D magnetic systems such as the 2D antiferromagnet K_2MnF_4 [60] and the out-of-plane 2D Heisenberg antiferromagnet presented in this study, $CrCl_3$ [13]. The pronounced shape of this curve with a maximum near lower angles, and a shallow minimum near θ = 55°, or the "magic" angle, has been observed in other systems and is a known feature of low-dimensional systems [60]. Just as the model described by (3), this $(3\cos^2\theta - 1)^2$-like behavior in Eq. 4 is a characteristic of 2D magnetic systems [13].

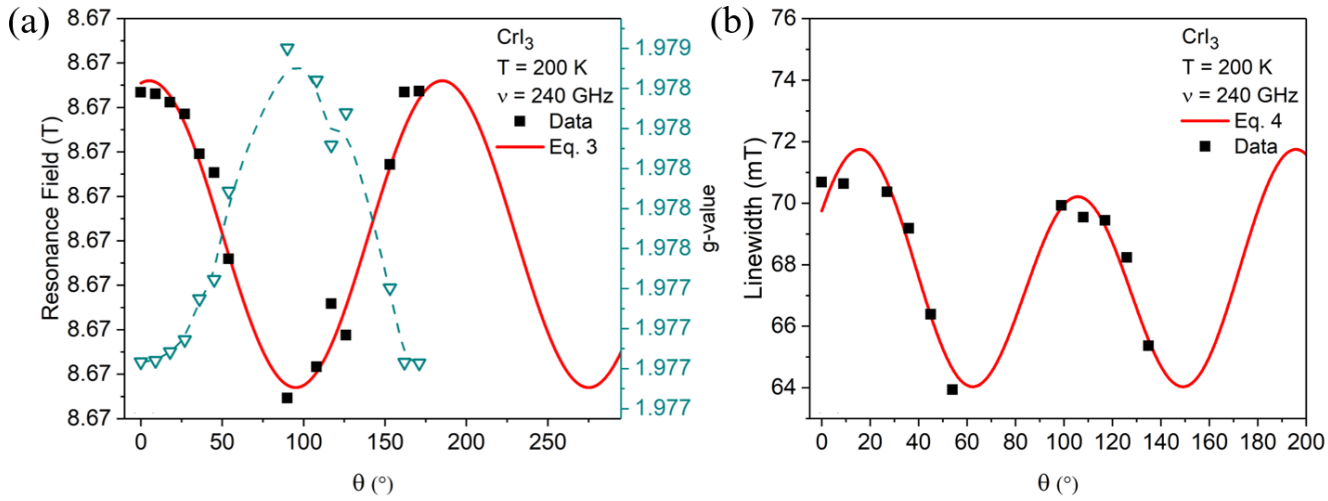

Figure 5.1: Angular dependence of the (a) resonance field and (b) linewidth collected from CrI_3 at $T = 200$ K fitted with a modified form of (3) and (4) to take into account a phase shift in Eq. 3: $H_{res}(\theta) = F[3\cos^2(\theta - \phi) - 1] + G$ and Eq. 4: $\Delta H(\theta) = A[3\cos^2(\theta - \phi) - 1]^2 + B$. The cyan data points in (a) show the calculated g-values with a B-spline to guide the eye and illustrate the inverse relationship between resonance field and g-value.

The applicability of these models are good indicators of two-dimensionality in our bulk sample, which we explain as the possible coexistence of antiferromagnetic correlations along with the dominant ferromagnetic correlations in bulk CrI_3. This induced two-dimensionality could be a consequence of an induced anisotropy by the applied magnetic field in the ESR experiment, pointing toward magnetic frustration within the 3D condensed matter system. This is especially important due to the fact that it has been theoretically predicted that an applied magnetic field is able to induce 2-dimensionality in the past [64]. It should also be pointed out that CrI_3 will exhibit interlayer antiferromagnetism in the bilayer, an indicator that some sort of magnetic frustration may carry into the bulk system [21].

Here, as these studies are ongoing, we have not discussed the temperature dependence of the ESR spectra from T = 200 – 4 K, nor the angular dependence of the ESR linewidth and resonance field in the ferromagnetic region at T = 4.4 K. Due to the structural and anisotropic similarities between CrI_3 and $CrBr_3$, as well as the known antiferromagnetic behavior in the bilayer,

there is good reason to believe that CrI_3 may exhibit many of the same behaviors observed in $CrBr_3$. We can say that with the application of Eq. 3 and Eq. 4, some sort of induced 2-dimensionailty exists within our system, and that the application of the BKT model would likely apply to CrI_3 as well. This is due to the presence of both FM and AFM correlations within the bulk sample, as well as a consequence of the spectrometer's applied magnetic field combined with the inherent anisotropy in CrI_3 that could lead to the induction of an effective 2D *XY* plane anisotropy in CrI_3 due to an interaction between the long-range spin vortices and spin clusters that may have been formed during magnetic phase segregation [21,42-44,46,61].

PART III: CONCLUSIONS

We have conducted high frequency ESR spectroscopy on the single crystal CrX_3 (where X = Cl, Br, I) as a function of temperature from $T = 200 – 4$ K and as a function of angle, θ, to gain insight into the effects of temperature, as well as the angular dependence of the linewidth and resonance field. Using various models and fits, we determine that the 3D van der Waals (vdW) ferromagnet $CrBr_3$ may exhibit 2D correlations by the Ginzberg-Landau critical model due to its adequate description of the temperature dependence of the ESR linewidth, indicative of the presence of 2D correlations. We also confirm that the in-plane ferromagnet and out-of-plane antiferromagnet $CrCl_3$, which is known to exhibit 2D Heisenberg and magnetic correlations suggestive of a weak *XY* model, follows the same behavior. This existence of competing magnetic phases is further revealed by the splitting between ZFC and FC magnetization measurements performed on $CrBr_3$. While direct experimental evidence for the long-range vortex-like correlations between spin clusters is not provided at this point, the analysis on the temperature dependent ESR linewidth using the BKT and critical model has led us to hypothesize that there is a formation of long-range vortex-like correlations between spin clusters. A similar conclusion has been made in a number of previous studies performed on Cr-based and low dimensional antiferromagnets [7-9,46]. Similar to the magnetic correlations recently discovered in CrI_3, this behavior, not commonly observed in layered vdW magnets, is thought to arise from the stacking structure and interlayer AFM correlations within the sample. Therefore, based on the experimental findings in previous reports [46,47], this BKT-like behavior is also understood to be a consequence of the spectrometer's applied magnetic field combined with CrX_3's characteristic anisotropy. With these findings, we have illustrated the importance of employing high sensitivity spectroscopy via ESR and suggest that CrX_3 may require additional follow-up investigations to better understand its magnetic correlations that likely extend to other layer-type vdW magnets.

REFERENCES

[1] I. Lee, F. G. Utermohlen, D. Weber, K. Hwang, C. Zhang, J. van Tol, J. E. Goldberger, N. Trivedi, P. C. Hammel, Phys. Rev. Lett. 124, 017201 (2020).

[2] J. Zeisner, A. Alfonsov, S. Selter, S. Aswartham, M. P. Ghimire, M. Richter, J. van den Brink, B. Büchner, V. Kataev, Phys. Rev. B 99, 165109 (2019).

[3] J. Zeisner, K. Mehlawat, A. Alfonsov, M. Roslova, T. Doert, A. Isaeva, B. Büchner, V. Kataev, Phys. Rev. Mat. 4, 064406 (2020).

[4] C. L. Saiz, M. A. McGuire, S. R. J. Hennadige, J. van Tol, S. R. Singamaneni, MRS Advances, 4(40), 2169-2175 (2019).

[5] S. R. Singamaneni, L. M. Martinez, J. Niklas, O. G. Poluektov, R. Yadav, M. Pizzochero, O. V. Yazyev, M. A. McGuire, Appl. Phys. Lett. 117, 082406 (2020).

[6] M. Hemmida, H.-A. Krug von Nidda, N. Büttgen, A. Loidl, L. K. Alexander, R. Nath, A. V. Mahajan, R. F. Berger, R. J. Cava, Y. Singh, D. C. Johnston, Phys. Rev. B 80, 054406 (2009).

[7] M. Hemmida, H.-A. Krug von Nidda, A. Loidl, J. Phys. Soc. Jpn. 80, 053707 (2011).

[8] M. Hemmida, H.-A. Krug von Nidda, A. Loidl, J. Phys.: Conf. Ser. 200 022016 (2010).

[9] M. Hemmida, H.-A. Krug von Nidda, V. Tsurkan, A. Loidl, Phys. Rev. B 95, 224101 (2017).

[10] J.F. Dillon, J. Appl. Phys. 33, 1191 (1962).

[11] M. S. Seehra, R. P. Gupta, Phys. Rev. B 9, 197 (1974).

[12] J. F. Dillon, C. E. Olson, J. Appl. Phys., 36, 1259 (1965).

[13] S. Chehab, J. Amiell, P. Biensan, S. Flandrois, Physica B 173, 211-216 (1991).

[14] C. Gong, L, Li, Z. Li, H. Ji, A. Stern, Y. Xia, T. Cao, W. Bao, C. Wang, Y. Wang, Z Q. Qiu, R. J. Cava, S. G. Louie, J. Xia, X. Zhang, Nat., 546, 265. (2017).

[15] B. Huang, G. Clark, E. Navarro-Moratalla, D. R. Klein, R. Cheng, K. L. Seyler, D. Zhong, E. Schmidgall, M. A. McGuire, D. H. Cobden, W. Yao, D. Xiao, P. Jarillo-Herrero, X. Xu, Nat. 546, 271 (2017).

[16] Adapted by permission from Springer Nature: [Cambridge University Press, MRS Advances, Electron spin resonance properties of CrI3 and CrCl3 single crystals, C. L. Saiz, M. A. McGuire, S. R. J. Hennadige, J. van Tol, S. R. Singamaneni, MRS Advances, 4(40), 2169-2175, COPYRIGHT (2019).

[17] M. Abramchuk, S. Jaszewski, K. R. Metz, G. B. Osterhoudt, Y. Wang, K. S. Burch, F. Tafti, Adv. Mater. 30, 1801325 (2018).

[18] T. A. Tartaglia, J. N. Tang, J. L. Lado, F. Bahrami, M. Abramchuk, G. T. McCandless, M. C. Doyle, K. S. Burch, Y. Ran, J. Y. Chan, F. Tafti, Sci. Adv. 6, 30, eabb9379 (2020).

[19] M. A. McGuire, H. Dixit, V. R. Cooper, B. C. Sales, Chem. Mater., 27, 612−620 (2015).

[20] P. Schmidt, M. Binnewies, R. Glaum, M. Schmidt, Chemical vapor transport reactions, Materials, modeling, Advanced topics on crystal growth, Ch. 9 pp. 227 – 305 (2013).

[21] W. Chen, Z. Sun, Z. Wang, L. Gu, X. Xu, S. Wu, C. Gao, Science. Vol. 366, 6468, pp. 983-987 (2019).

[22] N. D. Mermin, H. Wagner, Phys. Rev. Lett. 17, 1133 (1966).

[23] L. Capriotti, A. Cuccoli, A. Fubini, V. Tognetti, R. Vaia, Fundamental Problems of Mesoscopic Physics 203–216 (2004).

[24] H. Wang, V. Eyert, U. Schwingenschlogl, J. Phys. Condens. Mat. 23116003 (8pp) (2011).

[25] B. Huang, G. Clark, D. R. Klein, D. MacNeill, E. Navarro-Moratalla, K. L. Seyler, N. Wilson, M. A. McGuire, D. H. Cobden, D. Xiao, W. Yao, P. Jarillo-Herrero, X. Xu, Nat. Nanotechnology, 13, 544–548 (2018).

[26] D. Zhong, K. L. Seyler, X. Linpeng, R. Cheng, N. Sivadas, B. Huang, E. Schmidgall, T. Taniguchi, K. Watanabe, M. A. McGuire, W. Yao, D. Xiao, K. C. Fu, X. Xu, Sci. Advances, 3, e1603113 (2017).

[27] K. L. Seyler, D. Zhong, D. R. Klein, S. Gao, X. Zhang, B. Huang, E. Navarro-Moratalla, L. Yang, D. H. Cobden, M. A. McGuire, W. Yao, D. Xiao, P. Jarillo-Herrero, X. Xu, Nat. Phys. 14, 277 (2017).

[28] T. Song, X. Cai, M. W. Tu, X. Zhang, B. Huang, N. P. Wilson, K. L. Seyler, L. Zhu, T. Taniguchi, K. Watanabe, M. A. McGuire, D. H. Cobden, D. Xiao, W. Yao, X. Xu, Science, 360, 1214 (2018).

[29] D. R. Klein, D. MacNeill, J. L. Lado, D. Soriano, E. Navarro-Moratalla, K. Watanabe, T. Taniguchi, S. Manni, P. Canfield, J. Fernández-Rossier, P. Jarillo-Herrero, Science, 360, 1218 (2018).

[30] Z. Wang, I. Gutiérrez-Lezama, N. Ubrig, M. Kroner, M. Gibertini, T. Taniguchi, K. Watanabe, A. Imamoğlu, E. Giannini, A. F. Morpurgo, Nat. Communications 9, 2516 (2018).

[31] L. Lado, J. Fernández-Rossier, 2D Mater. 4, 035002 (2018).

[32] M. A. McGuire, G. Clark, Santosh K. C., W. M Chance, G. E. Jellison, Jr., V. R. Cooper, X. Xu, and B. C. Sales, Phys. Rev. Mat., 1, 014001. (2017).

[33] W.-B. Zhang, Q. Qu, P. Zhua, C.-H. Lam, J. Mat. Chem. C 3, 12457 (2015).

[34] J. W. Cable, M. K. Wilkinson, E. O. Wollan, J. Phys. Chem. Solids 19, 29 (1961).

[35] B. Kuhlow, Phys. Stat. Sol. A 72, 161 (1982).

[36] X. Yu, X. Zhang, Q. Shi, S. Tian, H. Lei, K. Xu, H. Hosono, Front. Phys. 14, 43501 (2019).

[37] Z. Zhang, J. Shang, C. Jiang, A. Rasmita, W. Gao, T. Yu, Nano Lett. 19, 5, 3138–3142 (2019).

[38] H. H. Kim, B. Yang, S. Li, S. Jiang, C. Jin, Z. Tao, G. Nichols, F. Sfigakis, S. Zhong, C. Li, S. Tian, D. G. Cory, G. Miao, J. Shan, K. F. Mak, H. Lei, K. Sun, L. Zhao, A. W. Tsen, Proceedings of the National Academy of Sciences 116 (23) 11131-11136 (2019).

[39] L. Webster, J. Yan, Phys. Rev. B 98, 144411 (2018).

[40] D. Ghazaryan, M. T. Greenaway, Z. Wang, V. H. Guarochico-Moreira, I. J. Vera-Marun, J. Yin, Y. Liao, S. V. Morozov, O. Kristanovski, A. I. Lichtenstein, M. I. Katsnelson, F. Withers, A. Mishchenko, L. Eaves, A. K. Geim, K. S. Novoselov, A. Misra, Nat. Electronics 1, pg, 344–349 (2018).

[41] B. Morosin, A. Narath, J. Chem. Phys. 40, 1958 (1964).

[42] G. T. Lin , X. Luo, F. C. Chen , J. Yan, J. J. Gao, Y. Sun, W. Tong , P. Tong, W. J. Lu, Z. G. Sheng, W. H. Song, X. B. Zhu, Y. P. Sun, Appl. Phys. Lett. 112, 072405 (2018).

[43] R. J. Cava, Phys. Rev. Lett. 91(13):137601 (2003).

[44] J. M. Kosterlitz, D. J. Thouless, J. Phys. C: Solid State Phys. 6 1181 (1973).

[45] V. L. Berezinskii, Sov. Phys. JETP 32, 493 (1971).

[46] A. Ashoka, K. S. Bhagyashree, S. V. Bhat, Phys. Rev. B. 102, 024429 (2020).

[47] A. Ashoka, K. S. Bhagyashree, S. V. Bhat, MRS Adv. 5, 2251–2260 (2020).

[48] L. J. De Jongh, Introduction to low dimensional magnetic systems pp. 1 - 47 (1990).

[49] Y. Yamasaki et al., 2D Mater. 4 041007 (2017).

[50] W. J. Hardy et al., Phys. Rev. B 91 054426 (2015)

[51] M. Arai et al., Appl. Phys. Lett. 107 103107 (2015).

[52] A. M. Goldman, pp. 135–160 (2013).

[53] D. J. Bishop and J. D. Reppy, Phys. Rev. Lett. 40 (1978).

[54] S. S. Rao, S. V. Bhat 2009 J. Phys. D: Appl. Phys. 42 075004 (2009).

[55] S. S. Rao, B. Padmanabhan, S. Elizabeth, H. L. Bhat, S. V. Bhat, J. Phys. D: Appl. Phys. 41, 155011 (2008).

[56] A. I. Shames, E. Rozenberg, G. Gorodetsky, A. A. Arsenov, D. A. Shulyatev, Y. M. Mukovskii, A. Gedanken, G. J. Pang, J. Appl. Phys. 91, 7929 (2002).

[57] V. Likodimos, M. Pissas, Phys. Rev. B 73, 214417 (2006).

[58] J. P. Joshi, S. V. Bhat, J. Magn. Res. 168, 284 (2004).

[59] E. A. Rozenberg, I. Shames, M. Auslender, G. Jung, I. Felner, J. Sinha, S. S. Banerjee, D. Mogilyansky, E. Sominski, A. Gedanken, Ya. M. Mukovskii, G. Gorodetsky, Phys. Rev. B 76, 214429 (2007).

[60] H. Benner, J. P. Boucher, pp. 323 - 378 (1990).

[61] S. Li, Z. Ye, X Luo, G Ye, H. H. Kim, B. Yang, S. Tian, C. Li, H. Lei, A. W. Tsen, K. Sun, R. He , L. Zhao, Phys. Rev. X 10, 011075 (2020).

[62] A. A. Kalenyuk, A. Pagliero, E. A. Borodianskyi, S. Aswartham, S. Wurmehl, B. Büchner, D. A. Chareev, A. A. Kordyuk, V. M. Krasnov, Phys. Rev. B 96, 134512 (2017).

[63] U. Tutsch, B. Wolf, S. Wessel, L. Postulka, Y. Tsui, H.O. Jeschke, I. Opahle, T. Saha-Dasgupta, R. Valentí, A. Brühl, K. Remović-Langer, T. Kretz, H.-W. Lerner, M. Wagner, M. Lang, Nat. Comm. 5, 5169 (2014).

[64] A. Cuccoli, T. Roscilde, V. Tognetti, R. Vaia, P. Verrucchi, Phys. Rev. B 67, 104414 (2003).

[65] P. M. Richards, M. B. Salamon, Phys. Rev. B 9, 32 (1974).

[66] K. Okuda, K. Kurosawa, S. Saito, M. Honda, Z. Yu, M. Date, J. Phys. Soc. Jpn. 55, pp. 4456-4463 (1986).

[67] Y. Cao, S. Cao, W. Ren, Z. Feng, S. Yuan, B. Kang, B. Lu, J. Zhang, Appl. Phys. Lett. 104, 232405 (2014).

[68] S. S. Rao, S. V. Bhat, J. Phys.: Condens. Matter 21 196005 (2009).

[69] Z. Hu, Z. Ma, YD Liao, H. Li, C. Ma, Y. Cui, Y. Shangguan, Z. Huang, Y. Qi, W. Li, Z. Y. Meng, J. Wen, W. Yu, Nat. Commun. 11, 5631 (2020).

[70] A. Kiel, Phys. Rev. B 12, 1868 (1975).

VITA

My name is Christian Lee Saiz. From an early age, my mom, an educator, instilled in me a love of natural sciences through science clubs she started at the elementary schools I attended. I had the privilege of becoming a teaching assistant at The University of Texas at El Paso (UTEP), where I was a laboratory instructor in the subjects of mechanics, electromagnetism, and astronomy. I also served as a physics tutor in the UTEP tutoring center focusing on any physics subject presented to me. I earned my Bachelor of Science degree in Physics with a minor in Mathematics from UTEP in May 2019. In the summer of 2019, before returning to UTEP to start the master's program, I was employed by El Paso Community College (EPCC) as a supplemental instructor where I taught pre-calculus workshops and served as a tutor in the math center covering a range of subjects from pre-calculus to calculus I - III.

When I arrived at UTEP in 2016 I immediately began working with Dr. Srinivasa Rao Singamaneni as a research assistant in the physics department. I have been tasked with managing every aspect of the laboratory. This included setting up and maintaining instrumentation, coordinating outreach activities, overseeing all chemicals that entered and left the facility, and training all students that joined the group. I have had the privilege of having my work presented at twelve scientific conferences around the United States. These works include over eleven poster presentations, presented by myself and others, and four oral presentations by myself. I was fortunate to be nominated for Best Poster Presentation in 2019 (MRS 2019) and was the winner of Best Oral Presentation in 2020 (MRS 2020). My first peer-reviewed publication was in 2018 entitled, "Electron spin resonance investigations on perovskite solar cell materials deposited on glass substrate". Since then I have co-authored eight manuscripts where I am first author on three.

Email address: clsaiz@miners.utep.edu